Time-resolved PIV for Aeroacoustic Source Analysis

David Breakey[1,*], John Fitzpatrick[1]

1: Department of Mechanical and Manufacturing Engineering, Trinity College Dublin, Ireland
* correspondent author: breakeyd@tcd.ie

Abstract Time-resolved Particle Image Velocimetry (TR-PIV) has become a valuable tool for spatio-temporally resolved flow measurements. Current camera and laser technology has advanced such that time domain events leading to sound generation can now be resolved over a reasonable spatial extent. In this paper, the use of TR-PIV is investigated for the analysis of aeroacoustic sources in two test cases, viz. a tandem cylinder pair subject to cross-flow and an open-jet. The localization technique employs the direct correlation $R_{u'p'}(\vec{x}_s, \vec{x}, \tau)$ of velocity fluctuations in the flow with pressure fluctuations outside of the flow region (Lee & Ribner 1972). The focus of this study is to determine the capacity of a TR-PIV setup to provide suitable estimates of $R_{u'p'}(\vec{x}_s, \vec{x}, \tau)$ and to examine how these space-time properties can be used for aeroacoustic noise source localization. The effect of aliasing inherent in the TR-PIV measurements on estimates of $R_{u'p'}(\vec{x}_s, \vec{x}, \tau)$ is considered by comparison to hot-wire anemometer (HWA) measurements. The suitability of the direct correlation method for the location of sound sources is then considered for the open-jet. In addition, a recently developed wavelet filtering technique (Grizzi & Camussi 2012) is used to separate the acoustic and hydrodynamic components of recorded near-field pressure signals. This enables a gain in the signal-to-noise ratio by eliminating the hydrodynamic component of pressure and thus improves estimates of the actual locations of acoustic sources in the flow. The technique is shown to provide a much cleaner correlation signal, enabling more physical interpretation of the potential noise sources. TR-PIV aliasing is shown to affect the measurement all turbulent properties in the frequency domain.

1. Introduction

Jet noise source localization techniques involving the correlation of in-flow fluctuations to far-field pressures have been used extensively since their introduction by Siddon (1970) and Lee & Ribner (1972). A key advantage of the technique is that the measured cross-correlation can be related analytically to a source term using Lighthill's acoustic analogy (1952, see § 2.1). Early investigations relied on intrusive probes such as hot-wire anemometers (HWAs) to measure time-resolved velocity fluctuations and microphones to measure the far-field pressure. The advantage of using a HWA is the high sample rates that are possible, which can well resolve the time-scales of the turbulence. However, HWAs provide information at a single point, meaning that large flow fields can only be recorded by traversing the probe and making several recordings, which are only correlated in time statistically. A second drawback is that introducing an intrusive probe into the flow field can also introduce a new source of sound. This source may be weak in comparison to the sound of the flow, but it will be highly correlated to the velocity fluctuations at the velocity probe, which can lead to erroneous correlation measurements (Richarz 1978). The intrusive aspect of HWAs was relieved in the 1970s by the introduction of the Laser Doppler Anemometer (LDA) at the expense of reduced time-resolution and a sample record that is intermittent. Despite early technological gains, correlation measurements were largely set aside until recently, with the introduction of more modern non-intrusive measurement techniques such as molecular Rayleigh scattering (Panda 2005). The technique has also been carried out in the frequency domain and combined with beamforming for the pressure measurements (Papamoschou et al. 2010) and to data from numerical simulations (Bogey & Bailly 2007).

The introduction of Particle Image Velocimetry (PIV) for spatially-resolved flow measurements has largely revolutionized the acquisition of data from flow experiments (Raffel et al. 2002), allowing large flow fields to be measured simultaneously. Until recently, this extensive spatial information has been obtained at the expense of time domain resolution with maximum PIV acquisition rates reaching only a few frames per second. Although these rates are sufficient for obtaining statistical information about

turbulence, they cannot resolve each flow realization in time, making it difficult to conclude what flow behaviour led to the observed statistics. Despite this limitation, Henning et al. (2010a, 2010b) were able to obtain cross-correlations between in-flow velocity fluctuations and far-field pressures in a number of flow configurations including a cylinder in cross-flow and a cold jet. This was achieved by coupling 5000 PIV measurements with a long series of high sample rate microphone measurements lasting over half an hour. Because of the low time resolution of the PIV recording, which is much smaller than the time-scale of the flow, each PIV image is essentially a separate realization of the flow. Thus the correlations are de-coupled from the particular events from each realization that led to the observed correlation value.

Recent developments in laser and camera technology have led to the introduction of Time Resolved-PIV (TR-PIV), where the acquisition rate is high enough to temporally resolve the flow field. The acquisition rate necessary to resolve a particular flow is dependent on the time-scales of the events to be resolved. In turbulence, very high acquisition rates are required to fully resolve the flow. Current equipment in common use is limited to acquisition rates around 10 kHz, while some limited tests have been carried out with reduced fields-of-view (FOVs) as high as 25 kHz (Bridges & Wernet 2007). Despite these high data rates, the discrete nature of PIV measurements introduces the problem of aliasing as it is impossible at present to pre-condition the turbulence data as the measurement of the flow velocity and the discrete sampling cannot be separated. This is because the PIV algorithm works by comparing two discrete images so there is no continuous signal and the use of anti-aliasing filters is impossible. This aliasing of high-frequency information into lower frequencies limits the accuracy of TR-PIV measurements in the frequency domain. This aliasing effect has been noted by previous investigators (Bridges & Wernet 2007), although its effect on the determination of the space-time correlation, $R_{u'p'}(\vec{x}_s, \vec{x}, \tau)$, and the frequency domain equivalents has not been investigated.

This primary aim of this paper is to investigate the ability of a TR-PIV setup to provide suitable estimates of $R_{u'p'}(\vec{x}_s, \vec{x}, \tau)$, as well as the frequency domain statistics of the flow and the utility of the knowledge of the space-time properties of this term for aeroacoustic noise source localization.

2. Theory

2.1 Direct Correlation Technique

The direct correlation technique seeks to quantify a relationship between the velocity fluctuations in a flow (the 'cause') and the observed pressure outside of the flow (the 'effect'). By applying Lighthill's analogy (1952) to a sound generation region of finite extent, and further using the directional simplification of Proudman (1952), Lee & Ribner (1972) showed that

$$R_{p'p'}(\vec{x}_s, \tau) = \frac{\rho_0}{4\pi c_0^2 r} \int \frac{\partial}{\partial \tau^2} R_{u_r u_r;p'}(\vec{x}_s, \vec{x}, \tau)\, d\vec{x}_s, \tag{1}$$

where[1]

$$R_{u_r u_r;p'}(\vec{x}_s, \vec{x}, \tau) = \langle u_r u_r(\vec{x}_s, t - r/c_0 + \tau) p'(\vec{x}, t) \rangle, \tag{2}$$

$\langle\,\rangle$ is the ensemble average, u_r is the fluid velocity component in the direction of the observer, p' is the fluctuating component of the pressure, ρ_0 is the ambient fluid density, c_0 is the ambient sound speed, and $\vec{x}_s$ and $\vec{x}$ are the positions of the source and observer, respectively. Also, $R_{qp}(\tau)$ is the cross-correlation function with time lag, τ, between $q(t)$ and $p(t)$ and $r = |\vec{x} - \vec{x}_s|$. By further invoking $u_r = \bar{u}_r + u_r'$, they concluded that

$$R_{u_r u_r;p'}(\vec{x}_s, \vec{x}, \tau) = \underbrace{2\bar{u}_r R_{u_r';p'}(\vec{x}_s, \vec{x}, \tau)}_{\text{Shear Noise}} + \underbrace{R_{u_r' u_r';p'}(\vec{x}_s, \vec{x}, \tau)}_{\text{Self Noise}}, \tag{3}$$

denoting the terms 'shear noise' and 'self noise' as above. This investigation will focus on the shear

[1] The semi-colon indicates that $u_r u_r$ is taken as a single quantity and correlated to p'.

noise component, $R_{u_r'p'}$, but in this case simplifying to the axial component of velocity, $R_{u_r'p'}$ for better comparison to the single-component hot-wire probe used. The correlations from the TR-PIV were also performed using u_r' and the result was largely the same with a higher noise level.

The conclusion of this formulation is that mapping regions of high correlation between any of the 'source' terms and the observed pressure is equivalent to mapping the sources for a particular observation location. Further, the maximum correlation should be observed when the time lag τ is equal to propagation time of sound from the source location to the observer location, or rather that the retarded time, $\tau_r = \tau - r/c_0 = 0$. This result assumes that the flow is quiescent and that the sources are compact (Lighthill's assumptions). Because the propagation paths of the sound will be slightly refracted by the mean flow, a small deviation in the peak location should be expected.

The correlation function, $R_{u'p'}$, is typically normalized by the energy of both u' and p' and called the correlation coefficient, $R_{u'p'}/(\sigma_{u'}\sigma_{p'})$, where σ_i is the root-mean-square of the data series. For discrete data series at two different acquisition rates, such as the case in this investigation, it is necessary to write the correlation as (Chatellier & Fitzpatrick 2005)

$$R_{u'p'}(\vec{x}_s, \vec{x}, k\Delta\tau) \approx R_{u'p'}[\vec{x}_s, \vec{x}, k] = \langle \frac{1}{N}\sum_{n=1}^{N} u'[n]p'[\alpha n + k] \rangle, \quad (4)$$

where α is the integer ratio between the pressure sample rate and the velocity sample rate. The time resolution of the correlation comes from the higher data rate signal, while the number of points averaged for each time lag (N), which influences the signal-to-noise ratio, comes from the lower rate signal.

2.2 Wavelet-based Pressure Signal Separation

A recent technique proposed by Grizzi & Camussi (2012) has used wavelets to separate pressure measurements taken in the near-field into hydrodynamic and acoustic components. Full details are presented in their paper, but a brief description is included here. Earlier attempts to separate the two components have been based on the wave-number based parameter of Arndt et al. (1997) and this has been established empirically. In practice, for measurements at a given location, this implies that all information above a specified wave-number is acoustic and all information below that frequency is hydrodynamic. However, this approach does not allow for analysis of the potential sources across the frequency range of the flow. The method of Grizzi & Camussi's is an extension of the wavelet de-noising technique used by Ruppert-Felsot et al. (2009). In this, the signal is filtered into a 'coherent' and an 'incoherent' part based on the magnitude of the wavelet coefficients of a discrete wavelet transform (DWT) being above a certain threshold. The refinement of Grizzi & Camussi is that the threshold level, having been estimated by the method of Ruppert-Felsot et al. (2009), is incremented and determined iteratively while monitoring several convergence criteria. These criteria are (a) the correlation peak of the hydrodynamic signal must correspond to a propagation velocity less than or equal to the flow velocity, (b) the correlation peak of the acoustic signal must correspond to a propagation velocity greater than or equal to the ambient sound speed, and (c) the peak ratio between the first and second peak of the hydrodynamic signal must be greater than a prescribed value representative of the signal to noise ratio.

The validity of wavelets to separate the two behaviours is not entirely certain a priori. However, the unique aspect of this technique is that in addition to a simple wavelet coefficient threshold for the separation, the apparent propagation velocity of the resulting signals is used in the separation criteria. This is important because acoustic behaviour in a flow can be defined as those fluctuations that propagate at the sound speed, while all other fluctuations should be considered hydrodynamic. Therefore a technique that incorporates this convection property in the separation seems to be the best separation method currently available. Of course, the true validity can only be affirmed if the signals exhibit behaviours that correspond to those expected for each component which is true for the results presented by Grizzi & Camussi (2012). Particularly interesting is their observation of the 'cone of silence' in the low emission angles of the near-field. These results lend support to the validity of the use of this separation technique in these tests. Also, since the acoustic fluctuations decay with observation distance,

this separation technique should allow higher signal-to-noise ratios because acoustic measurements can be taken closer to the jet. This is particularly important when testing subsonic jets that have low overall noise emissions.

The technique, however, does suffer drawbacks. The first of these being that it becomes less efficient when the energies of the acoustic and hydrodynamic fluctuations are similar in magnitude so that the threshold does not necessarily clearly separate the two behaviours. For the second, the technique becomes inefficient as the speed of the jet approaches or exceeds the sound speed. In this case, there is no longer a clear separation between the propagation speeds of the sources resulting in blurring the line between the two behaviours making separation difficult.

3. Experiment Setup

The experiment consisted of two setups with a base flow provided by the open-jet facility described by Chatellier and Fitzpatrick (2005). In the first setup a tandem cylinder pair was inserted into the jet flow as a stationary, high-volume sound source. The purpose of this was to test the technique with a relatively simple sound source distribution. The second setup applies the same technique to a standard open-jet. A full schematic of each setup is provided in figure 1. The diameter of the jet, D_{Jet}, was 50.8 mm while the diameters of the cylinders, D_{Cyl}, were both 6 mm. The centre of the second cylinder was used as the coordinate reference and located at 1.46 D_{Jet} from the nozzle lip. In both cases, the jet was operated at $U_{Jet} = 85$ m/s. The measurements were carried out at a number of relevant areas of interest (AOIs). For the cylinders, this was one AOI around the cylinders, and a second in their wake. For the jet, AOIs with a 5 mm overlap extended from the nozzle lip to $6.6D_{Jet}$, extending beyond the end of the potential core, which ended at $5.5D_{Jet}$. The microphones were located at $x = 3.54D_{Jet}, y = 2.5D_{Jet}$ for the tandem cylinders and $x = 7D_{Jet}, y = 4D_{Jet}$ for the jet. In both cases the separation distance between the microphones was 21 mm. The dominant vortex shedding frequency of the tandem cylinder pair was 1.9 kHz, which was considered to be well-resolved by the TR-PIV measurements obtained at 7.5 kHz. The TR-PIV for the open-jet case was obtained at 9 kHz. The Reynolds numbers of the cylinders based on cylinder diameter and the jet based on jet diameter were 3.5×10^4 and 2.9×10^5, respectively. The turbulence characteristics of this jet have already been studied extensively (Kennedy 2010).

The PIV system employed for these tests included a Quantronix Darwin Duo (15 mJ/pulse @ 1 kHz) dual-cavity laser capable of repetition rates of up to 10 kHz per oscillator. A LaVision HighSpeedStar 6 camera with 8 GB of onboard memory capable of 5400 fps at full frame (1024 px × 1024 px). PIV processing was carried out using LaVision DaVis 7.2 software using a multi-pass approach with a final window size of 32 × 32 pixels and 50% overlap. This gave a final vector spacing of ≈1.1mm for both tests. To obtain a higher framing rate, it was necessary to reduce the FOV as indicated in figure 1. The camera memory allowed the storage of 12148 images pairs per AOI for the cylinder case and 10914 image pairs for the jet. The microphone system used GRAS components including two 1/4" 40BH microphones connected to 26AC preamplifiers and a 12AN power module. The HWA measurements were made with a Dantec 90C10 constant temperature anemometry module using a single-component probe (type 55P11) oriented so that it measured the axial component of the flow velocity. The analogue signals were sampled with LabVIEW software using an NI PXI-4472B card, which has built-in anti-aliasing filters set to a cut-off of $0.48\, f_s$. The HWA measurements in the open-jet test were made from $2 - 4D_{Jet}$ in increments of $0.2D_{Jet}$ as a means to compare the PIV results with the HWA. The PIV and HWA measurements were not carried out simultaneously. The cross-correlations and power spectra were obtained using blocks of 256 points with 25% overlap, yielding 63 averages for the cylinder case and 56 for the jet. The corresponding frequency resolutions were 30 Hz, and 35 Hz, respectively. In the presented spectra and coherences, two iterations of 3-point Hanning smoothing were also applied. No smoothing was performed on the cross-correlations.

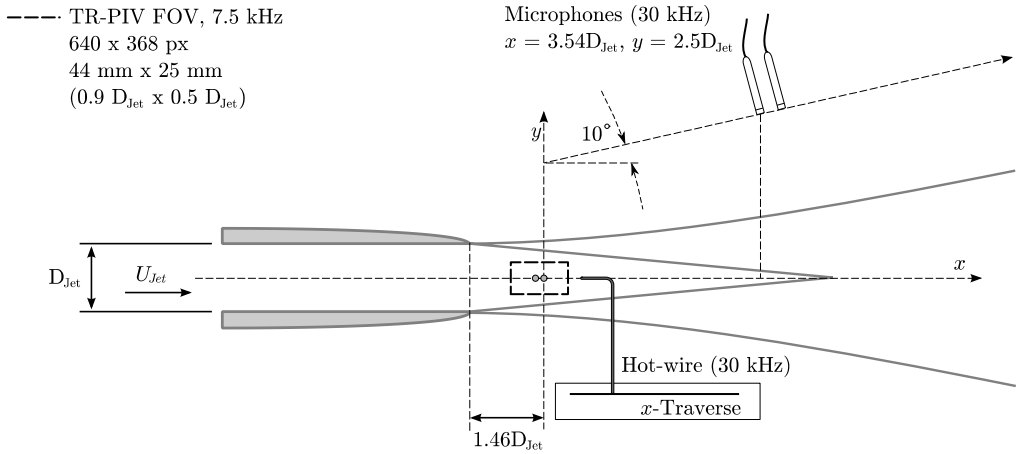

(a) Tandem cylinder pair setup.

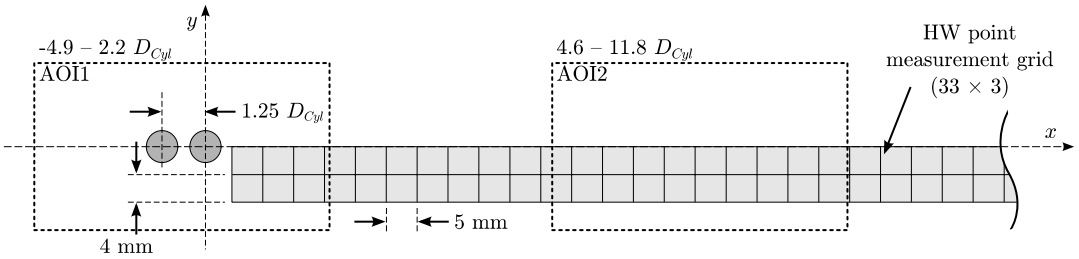

(b) Close-up of tandem cylinder pair velocity measurements

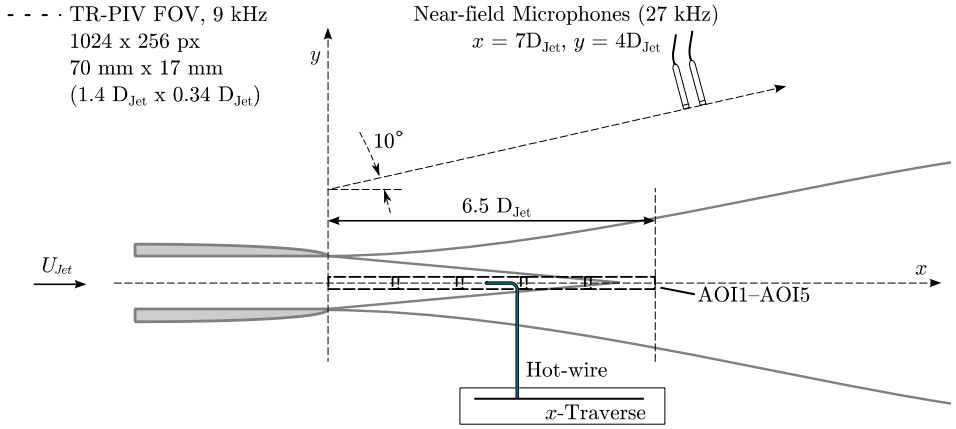

(c) Open-jet flow measurements

Figure 1: Experiment setup.

4. Results and Discussion

4.1 Wavelet Separation

Figure 2(a) shows the ability of the wavelet algorithm to separate the components of the pressure signal. The spectra match the expected shapes for the separation with the signal above a certain cut-off dominantly appearing as acoustic while below the cut-off the energy is dominantly hydrodynamic. For reference, the empirically derived cut-off of Arndt et al. (1997) is plotted for each case. Contrary to the criteria of Arndt et al., the non-dominant signal can be retrieved even though it energy is orders of magnitude below the dominant signal beyond the cut-off. The location of the cut-off from the wavelets corresponds well with the criteria of Arndt et al. This result is similar to those reported by Grizzi & Camussi (2012) when they introduced this technique.

Pertinent to the current analysis is the comparison between the correlations obtained by using the filtered and unfiltered signal shown in figure 2(b). The correlation signal from the filtered acoustic signal is significantly higher than from the total signal. This results in an increase in signal-to-noise ratio when

using this technique. Additionally, the hydrodynamic component of the signal is barely correlated with the velocity fluctuations. This is especially useful for the current jet investigation because the total noise output from such a low-speed jet is relatively low.

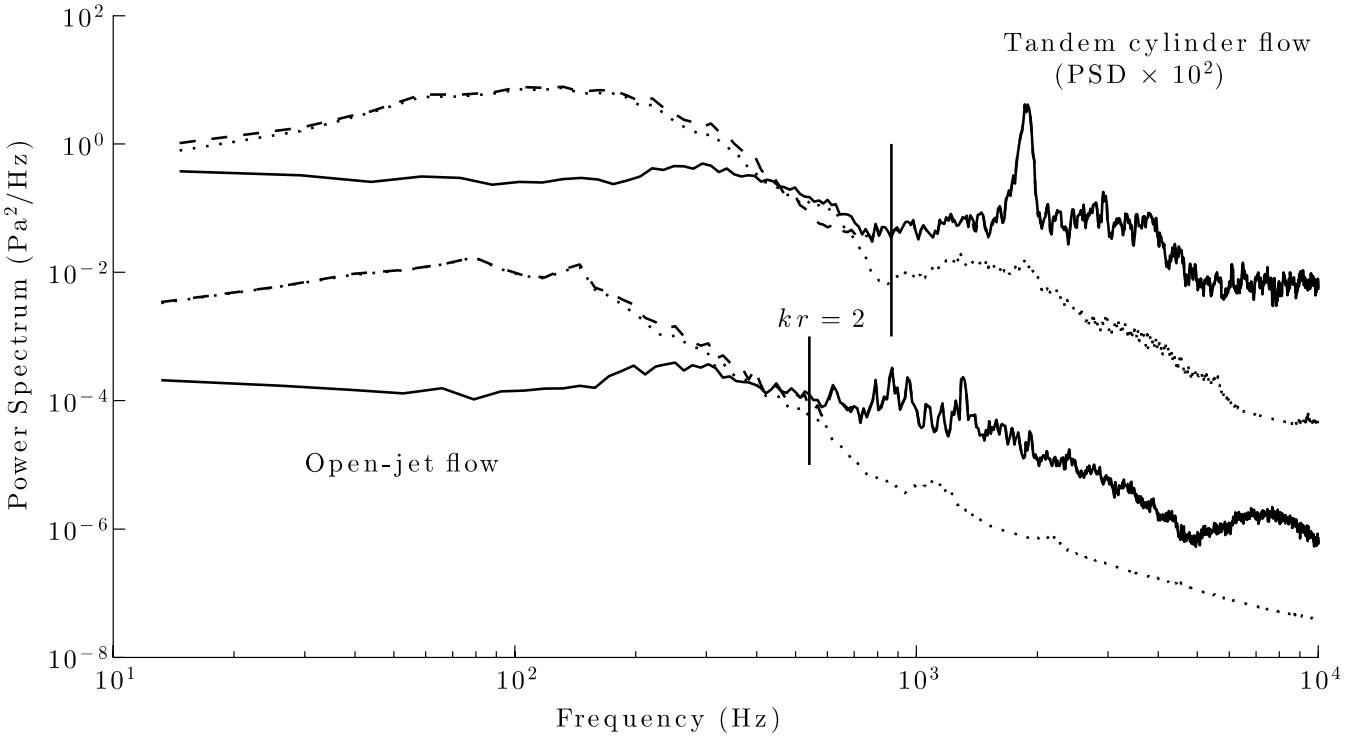

(a) Pressure spectra of each pressure component. $kr = 2$ is indicated for each microphone location. The tandem cylinder curve is shifted up by a factor of 102 for clarity.

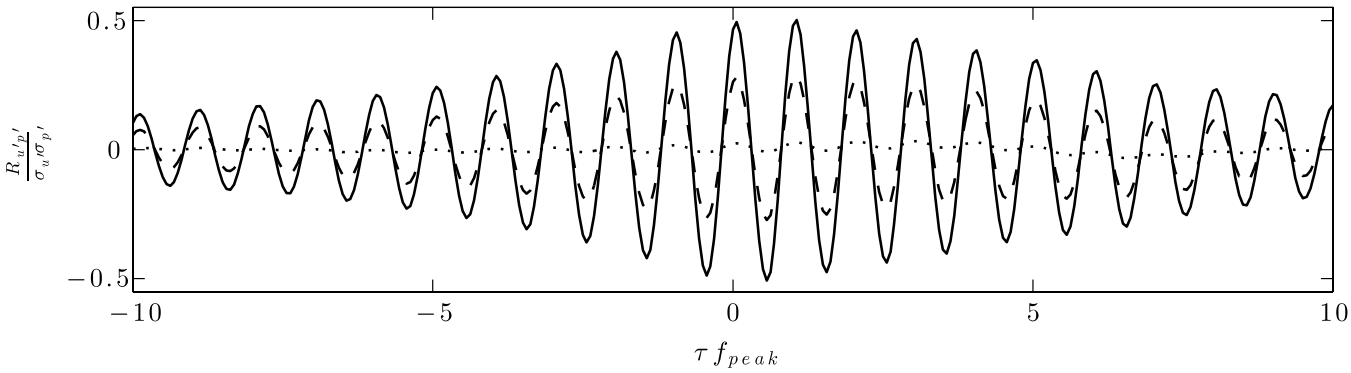

(b) Comparison between correlations of u' (HWA) and each p' component behind tandem cylinders at $x = 1.9D_{Cyl}, y = -1.3D_{Cyl}$.

Figure 2: Wavelet filtering of microphone signals in jet near-field. – – – Total pressure signal, ——— Acoustic component, ····· Hydrodynamic component.

4.2 Tandem Cylinders

Figure 3 presents a summary of the time and space resolution for the TR-PIV in the tandem cylinder test case. Figure 3(a) shows that the correlation map in the wake of the cylinder is characteristic of vortex structures, a result consistent with the vortex shedding behind the cylinders at the same frequency as the sound source from the cylinders. Since the fluctuating forces acting on the cylinders are associated with this vortex shedding, the dominant sound source is of dipole nature, and the shed vortices are well correlated to the sound. It can be clearly seen that the TR-PIV shows the same underlying structure as the HWA measurements but with better spatial resolution, indicating the cross-correlation coefficient is well-resolved in space. Figures 3(b) & (c) compare the power spectra obtained at two x-locations behind the cylinders and there is good agreement for the peak corresponding to the vortex shedding frequency but the agreement is not so good at higher and lower frequencies where the TR-PIV seems to

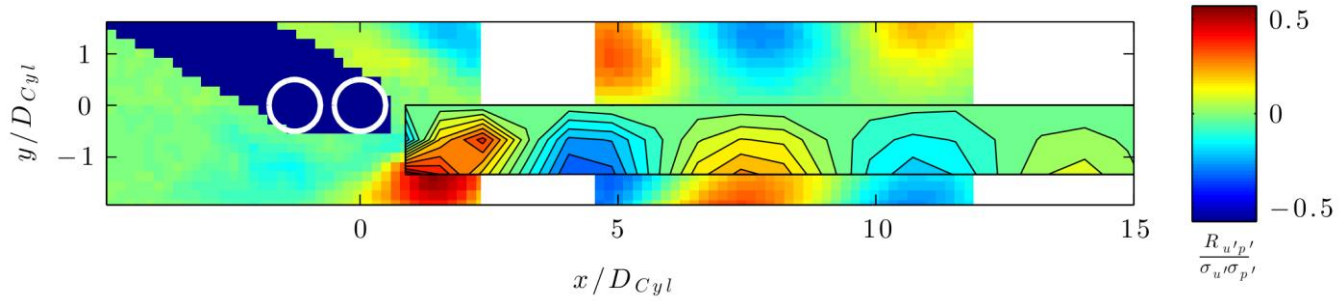

(a) Snapshot of cross-correlation at $\tau f_{\text{peak}} = 1.13$. (HWA measurements are boxed section.)

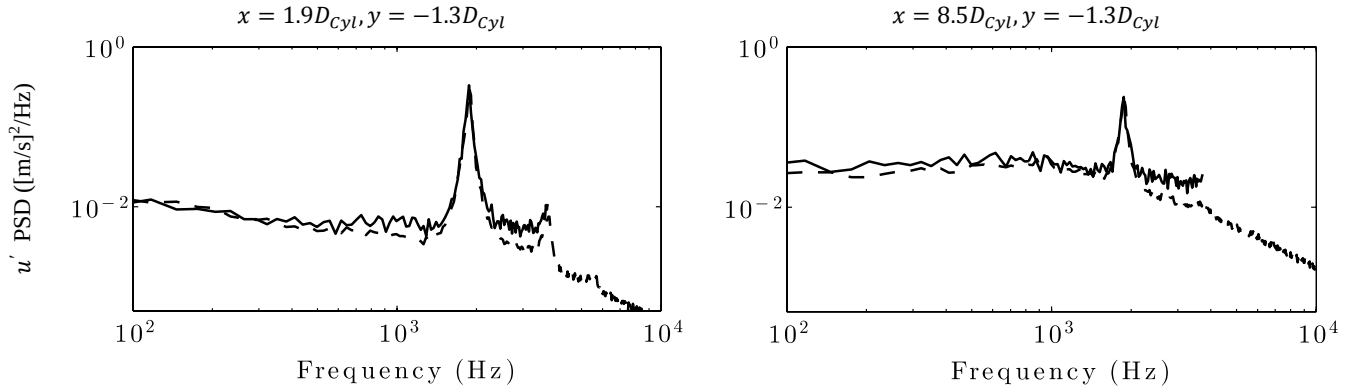

(b)

(c)

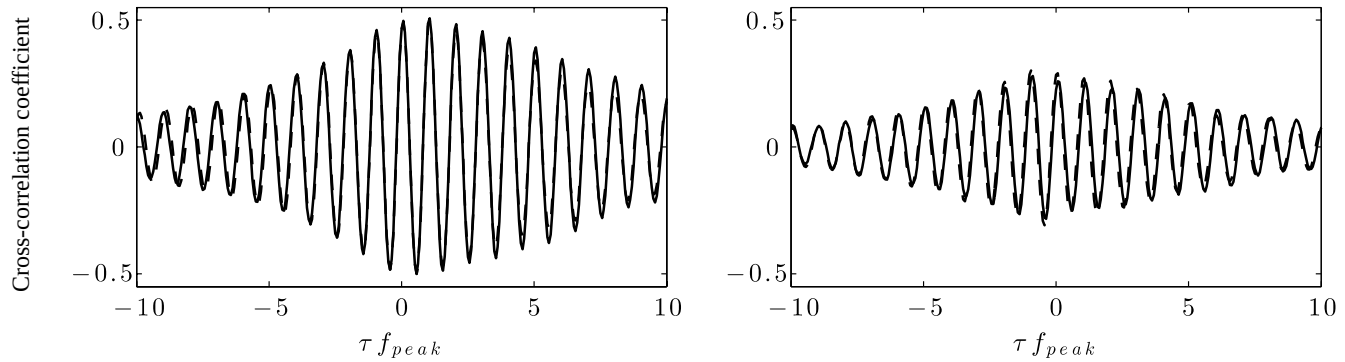

(d)

(e)

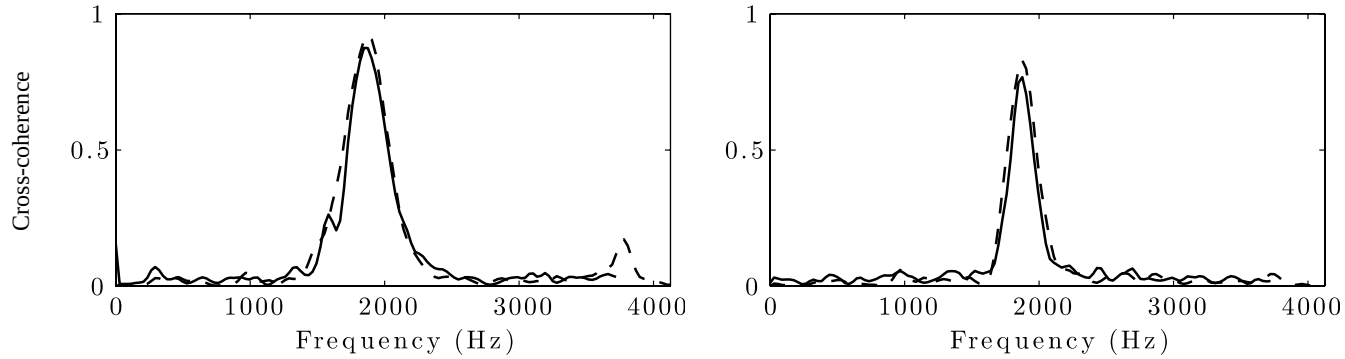

(f)

(g)

Figure 3: Comparison between space-time resolution of TR-PIV and HWA-based $u'p'$ correlation quantities. For (b)-(g) ——— TR-PIV, – – – HWA. For (d) & (e) $f_{peak} = 1.9$ kHz.

overestimate the spectrum. At high frequencies this can be associated with aliasing, which occurs well below the Nyquist frequency of 3.75 kHz and can be explained on the grounds described in § 1. Though even at frequencies below the well-resolved peak the TR-PIV appears aliased when the flow energy is low. For the time domain results in figures 3(d) & (e), there is very good agreement in shape, amplitude, and phase of the curves, even when aliasing is present in the frequency domain. Figures 3(f) & (g) show that the aliasing has an effect on the coherence, even at the edges of the vortex shedding peak, where the power spectrum was reasonably resolved. Unfortunately, since the source investigated is not highly coherent in the range where aliasing is dominant, it is not possible to tell if this would significantly reduce the coherence in this range.

4.3 Open-jet

Figure 5 shows the TR-PIV power spectra of u' measured along the jet centre-line and compared to HWA. The maximum power of around 1000 Hz can be observed near the end of the potential core of the jet where there is high fluctuation energy. However, close to the nozzle no fluctuations are resolved, and the noise floor is evident. As was the case in § 4.2, for all xs considered, the spectrum levels out at high frequencies rather than decaying continuously, indicating the presence of aliasing. Figure 5(a) indicates the time domain correlation signature measured on the centre-line of the jet is characterized by a dominant oscillation frequency of 1190 Hz corresponding to a Strouhal number based on a convection velocity of $fD_{Jet}/U_c \approx 1$. This frequency is close to the peak power of u' and represents the dominant instability of the jet in the potential core. The space-time correlation peaks are also extended over an axial extent of $\approx 4D_{Jet}$. This distance is significantly greater than the lip-line integral hydrodynamic length scale of $0.6-0.8D_{Jet}$ reported for this jet by Kennedy (2010). The location of $\tau_r = 0$ is indicated in figure 5(a) by a thin dashed line and represents the expected time lag for the correlation peaks if a Lighthill-type model of sound production by uncorrelated eddies was applied. However, here the peaks fall on a common line with a negative slope. Henning et al. (2010b) reported similar results previously and explained the peak signature by assuming that the main sound source is at the nozzle lip and observed that peaks downstream only represent correlation to the lip source rather than independent sound production. For the case of downstream fluctuations correlated to an upstream source, the time lags of the correlation peak can be predicted by modelling the system as in figure 6. Here, an upstream fluctuation $q_{s1}(t)$ originates somewhere in the jet flow and is then convected downstream at U_c. After some time, η/U_c, the fluctuation is $q_{s2}(t-\eta/U_c)$. If q is measured at both locations, there will be a significant correlation between q and p at both x-locations. The geometry of the model gives the expected peaks at:

$$\tau_{r,peak} = \tau_{s1,p} - \tau_{s2,p} - \eta/U_c, \qquad (5)$$

where η is the distance between the sources, U_c is the convection velocity, and $\tau_{s1,p}$ and $\tau_{s2,p}$ are

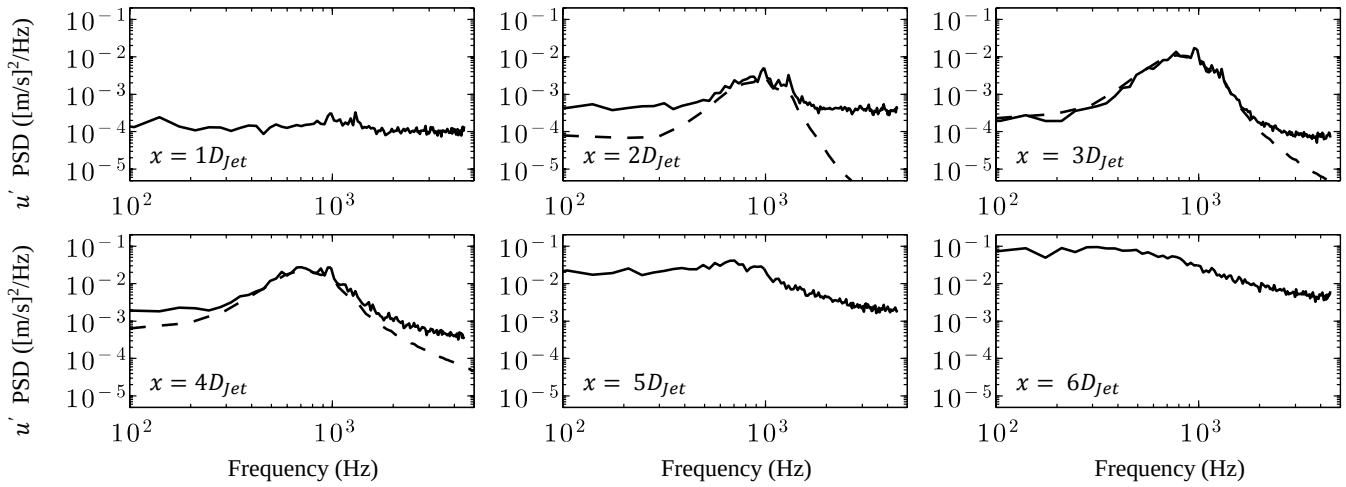

Figure 4: u' TR-PIV and HWA power spectra. ——— TR-PIV, – – – HWA. (HWA spectra available only for $x = 2-4D_{Jet}$.)

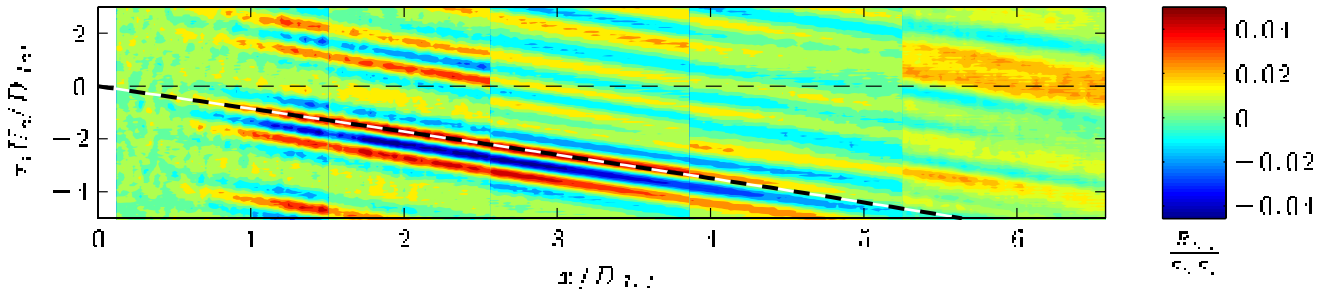

(a) Experimental open-jet centre-line correlations

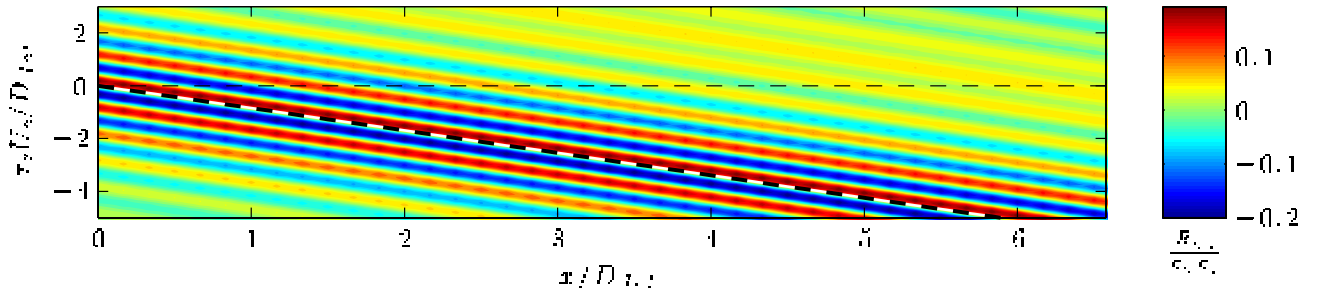

(b) Simulated correlation trace

Figure 5: Cross-correlation coefficients between u′ and the acoustic part of p′ separated by the wavelet method. The thin dashed line is $\tau_r = 0$, and the thick dashed line represents the expected peak locations based on a convected source model (see figure 6).

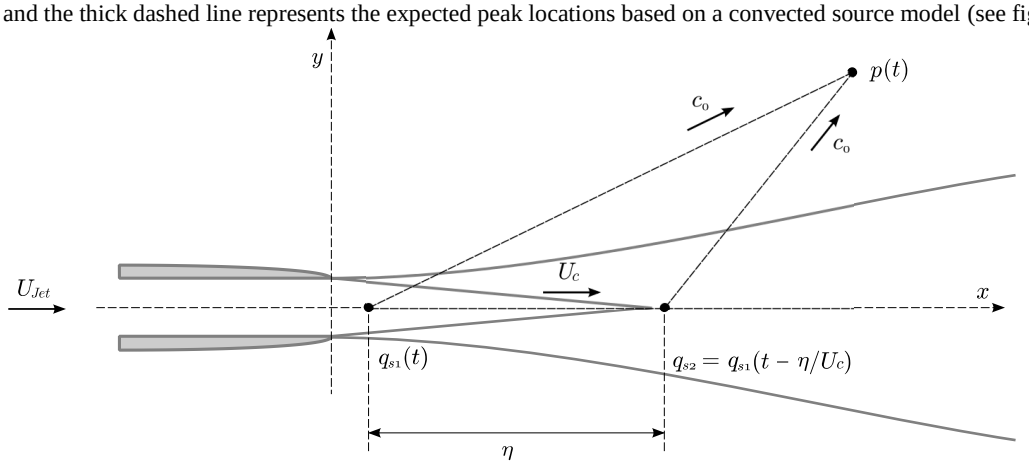

Figure 6: Source model for correlation simulation.

the propagation times from q_{s1} and q_{s2} to the observer location. The convection velocity was obtained from the slope of the peaks of the space-time correlation of u' at $U_c = 0.7U_{Jet}$. The line from equation (5) is plotted as a thick dashed line in figure 5(a) with $x_{s1} = 0$, and the agreement is evident.

However, this correlation signature does not prove that the lip fluctuation is the dominant noise source, and true source localization is ambiguous. A simple numerical simulation with an analytical sound source can illustrate this. Consider a line source representing a distribution of correlated monopoles on the axis of the jet that has a strength per unit length described by[2]

$$q(x,t) = \partial^2 T_{ij}(x,t)/\partial x_i \partial x_j = A\cos\left[2\pi f\left(t - \frac{x}{U_C}\right)\right]\exp\left[-\left|t - \frac{x}{U\_C}\right|/t_c\right], \qquad (6)$$

where A is the amplitude, f is the oscillation frequency, x is the axial position, t_c is a characteristic time scale of the source, and U_c is the convection velocity. The so-called Lighthill stress tensor is given by $T_{ij}(x,t)$. Such a source is similar to, for example, a convecting instability wave, or wave packet as described by Cavalieri et al. (2010). Now, assume that the received emissions at an observer location are somehow damped and this damping is dependent on the source position. This could be possible if there

[2] $q(x,t) = \delta(y)\delta(z)q(\vec{x},t)$

was a region of high sound absorption between the source location and observer, or if some of the acoustic energy were refracted away from the particular observation location by the mean flow. This damping envelope was proposed in this case as the sum of two separated Gaussians:

$$D(x) = B\exp[-(x-x_{s1})^2/b^2] + C\exp[-(x-x_{s2})^2/c^2]. \quad (7)$$

The parameters for the simulation were selected to mimic the current experiment and are presented in table 1. x_{s1} was chosen as the nozzle lip, and x_{s2} was a location near the end of the potential core.

Table 1: Source simulation parameters

$A = 1$	$t_c = 0.001$	$U_c = 85$ m/s	$f = 1190$ Hz
$B = C/10$	$C = 1$	$b = 100$	$c = 100$
$x_{s1} = 0D_{Jet}$	$x_{s2} = 6D_{Jet}$		
$-18\ D_{Jet}/U_c < t < 18\ D_{Jet}/U_c$	$0 < x < 10D_{Jet}$	$f_s = 27$ kHz	$dx = D_{Jet}/6$

To simulate strong source activity at x_{s2} and weaker activity at x_{s1}, C was 10 times greater than B. The true local source strength (in the sense of sound received by the observer) is then $q_t(x,t) = q(x,t)D(x)$. The observed sound can be calculated by Lighthill's analogy (1952) using a free-space Green's function as

$$p(t) = \frac{1}{4\pi r}\int_0^\infty q(x, t - r/c_0)D(x)dx. \quad (8)$$

$q(x,t)$ and $p(t)$ can now be correlated directly. Since the correlation is normalized by the local signal strength and the modulation $D(x)$ is constant in time, the result is the same as that obtained using $q_t(x,t)$. Time series of $q(x,t)$ were created for each point on a grid with a spacing of dx and a sample rate of f_s. The oscillation frequency, f, was chosen to correspond to the main oscillations in figure 5(a). A contribution to the far-field pressure for each grid point was then calculated independently by shifting each $q(x,t)$ by r/c_0 and multiplying by $1/4\pi r$. The shift was effected by passing $q(x,t)$ into the frequency domain, multiplying by $e^{-2j\pi f\phi r/c_0}$, and returning to the time domain. The observation location was that of the first microphone from the experiment. Each contribution was then multiplied by $D(x)$ and all the contributions were summed and multiplied by dx at each time step.

Figure 5(b) indicates the similarity between the experimental correlations and the simulated ones with the peaks of the correlation still predicted by equation (5). The result is consistent with the presence of axially extended, coherent structures as the sound source in the jet, but the time domain correlation cannot prove this unambiguously. It is clear, however, that the fluctuations on the centre-line related to the emitted sound have a correlation length much longer than the traditional integral hydrodynamic length scale measured on the lip-line, indicating the fluctuations related to noise emissions may be more organized on the centre-line. When the correlation is dominated by a single frequency and the source is correlated over a large axial extent, the cross-correlation technique fails to uniquely locate the strongest source activity. It is not surprising that the dominant correlation is recorded in the frequency range where TR-PIV best resolves the u' signal. For higher fidelity over a broader frequency range, it will be necessary to deal with the problem of aliasing in TR-PIV.

5. Conclusions

TR-PIV has been shown to be an effective tool for identifying the same correlation features available with traditional single-point measurement techniques such as HWA. The advantage of TR-PIV in this case is that the results are resolved both in time and space for each flow realization as opposed simply to ensemble averages. This will enable future efforts to focus on how individual flow realizations contribute to sound emission, an essential component of noise reduction schemes.

Aliasing is an important consideration in TR-PIV measurements. A tandem cylinder configuration in a jet flow has shown that aliasing in the TR-PIV time series does significantly affect the calculation of the turbulent properties as the signal to noise (aliasing) ratio is high. It has been shown that aliasing will

affect the estimation of all turbulent properties in the frequency domain especially at higher frequencies. It may be possible to use the coherence function as a correction for the aliasing, but this will require further study.

The results for the cross-correlations in the open-jet case indicate that the localization of sound sources is complicated by the mutual correlation of fluctuations, which appear to convect with the flow. A simple model was proposed and validated for how axially extended, convected flow fluctuations originating at the nozzle can explain the observed correlation signature without requiring the main source location to be at the nozzle lip. The high correlation values observed far downstream indicate that the traditional hydrodynamic integral length scale appears to underestimate the correlation length of the sound-generating components of the flow, which may only account for a small portion of the total flow energy. It also remains to be seen exactly what the effect of aliasing across the flow field has had on these "surprising" results.

As the technique is further refined, the spatial nature TR-PIV will yield critical information about the distribution and behaviour of aeroacoustic sound sources. In order to achieve this, it will be necessary to develop techniques to extract the acoustically important components of the raw velocity signal and to treat the problem of aliasing.

6. Acknowledgements

This work was supported by Science Foundation Ireland under contract number 09/RFP/ENM2469. The first author was also supported by a Natural Sciences and Engineering Research Council of Canada postgraduate scholarship.

7. References

Arndt RE, Long DF, Glauser MN (1997) The proper orthogonal decomposition of pressure fluctuations surrounding a turbulent jet. J Fluid Mech 340:1–33.

Bogey C, Bailly C (2007) An analysis of the correlations between the turbulent flow and the sound pressure fields of subsonic jets. J Fluid Mech 583:71–97.

Bridges J, Wernet M (2007) Effect of Temperature on Jet Velocity Spectra. NASA Glenn Research Center, Cleveland, Ohio, NASA/TM—2007-214993; AIAA-2007-3628.

Cavalieri AVG, Jordan P, Gervais Y, Agarwal A (2010) Jittering wave-packet models for subsonic jet noise. In Proceedings of the 16th AIAA/CEAS Aeroacoustics Conference, Stockholm, Sweden, 2010.

Chatellier L, Fitzpatrick J (2005) Spatio-temporal correlation analysis of turbulent flows using global and single-point measurements. Exp Fluids 38:563–575.

Grizzi S, Camussi R (2012) Wavelet analysis of near-field pressure fluctuations generated by a subsonic jet. J Fluid Mech 698:93–124.

Henning A, Koop L, Ehrenfried K (2010a) Causality correlation in aeroacoustic experiments by means of simultaneous PIV and microphone-array. In Proceedings of the 3rd Berlin Beamforming Conference, Berlin, Germany, 2010.

Henning A, Schröder A, Krebs I, Agocs J (2010b) Aeroacoustic investigations on a cold jet by means of simultaneous PIV and microphone measurements. In Proceedings of the 15th International Symposium on Applications of Laser Techniques to Fluid Mechanics, Lisbon, Portugal.

Kennedy J (2010) The influence of chevrons on the turbulent characteristics of jets. PhD Thesis, Trinity College Dublin.

Lee HK, Ribner HS (1972) Direct correlation of noise and flow of a jet. J Acou Soc Am 52:1280-1290.

Lighthill MJ (1952) On sound generated aerodynamically: I. General theory. In Proceedings of the Royal Society A: Mathematical, Physical and Engineering Sciences 211:564–587:

Panda J (2005) Identification of noise sources in high speed jets via correlation measurements: a review.

NASA Glenn Research Center, Cleveland, Ohio, NASA/CR—2005-213817.
Papamoschou D, Morris PJ, Mclaughlin DK (2012) Beamformed flow-acoustic correlations in a supersonic jet. AIAA J 48:2445–2453.
Proudman I (1952) The generation of noise by isotropic turbulence. In Proceedings of the Royal Society A: Mathematical, Physical and Engineering Sciences 214:119–132.
Raffel M, Willert C, Wereley S, and Kompenhans J (2002) Particle image velocimetry: a practical guide. Springer, Berlin.
Richarz WG (1978) Direct correlation of noise and flow of a jet using laser doppler. University of Toronto Institute for Aerospace Studies, Toronto, UTIAS Report 230.
Ruppert-Felsot J, Farge M, Petitjeans P (2009) Wavelet tools to study intermittency: application to vortex bursting. J Fluid Mech 636:427–453.
Siddon TE (1970) Surface dipole strength for flow past airfoils. J Acou Soc Am 48:75.